Journal of Natural Resources and Farming
https://doi.org/10.7770/jonraf-v2-art2904

JONRAF Journal of Natural Resources and Farming

SPECIAL ISSUE

From classical phenological models to reaction–diffusion equations: A spatial bioclimatic framework for cherry phenology

William Campillay-Llanos[a*], Marlon M. López-Flores[b], Samuel Ortega-Farías[c]

Núcleo de Investigación en Producción Alimentaria, Facultad de Recursos Naturales, Universidad Católica de Temuco, Temuco 4813302[a], Chile
Artificial Intelligence, Robotics and Cybernetics Laboratory (LIARC), Military Institute of Engineering, Rio de Janeiro[b], Brazil
Research and Extension Center for Irrigation and Agroclimatology (CITRA) and Research Program on Adaptation of Agriculture to Climate Change (PIEI A2C2), Universidad de Talca, Campus Lircay, Talca[c], Chile

Article history
Received: 10/02/2026
Accepted: 09/09/2026
Published: 22/09/2026

Corresponding author
*William Campillay-Llanos
williamcampillay@gmail.cl

ABSTRACT
Thermal-time models are widely used to predict fruit-tree phenology, but most operational formulations describe only temporal development and assume that an orchard is spatially homogeneous. This assumption can conceal within-orchard asynchrony caused by microclimate, topography, soil properties, canopy structure, and management. We propose a spatial extension of the classical monomolecular phenological model for sweet cherry (Prunus avium L.) using a reaction–diffusion equation. The reaction term represents local physiological development as a function of accumulated growing degree days (GDD), whereas the diffusion term provides an effective spatial coupling between neighbouring orchard sectors. One- and two-dimensional formulations are considered, with a bounded space–time development rate that accommodates persistent gradients and management zones. The equations are solved by an implicit-explicit finite-difference scheme in which reaction is treated explicitly and diffusion implicitly. Simulations based on thermal conditions from the Maule Region of Chile reproduce smooth but persistent intrafield phenological gradients. Warming scenarios advance phenological development at the same calendar date and may amplify differences among orchard sectors, particularly at later stages. The framework connects established thermal-time models with spatial process modelling and provides a basis for zone-specific irrigation, crop protection, and harvest planning.

Keywords: Sweet cherry; growing degree days; phenological modelling; reaction-diffusion equation; spatial heterogeneity; climate change.

1. Introduction

Phenology regulates critical decisions in fruit production, including frost protection, irrigation, pesticide application, pollination management, and harvest scheduling. In sweet cherry, shifts in budbreak, flowering, and fruit maturity can directly affect yield, fruit quality, and exposure to climatic hazards. Projected warming in central and south-central Chile is therefore expected to alter both the rate of thermal accumulation and the calendar dates of key developmental stages.

Growing degree-day models provide an interpretable connection between temperature and crop development. Monomolecular and related nonlinear models have a long history in Mediterranean fruit production. For example, Ortega-Farías et al. (2002) developed predictive models of phenology and maturity evolution for Cabernet Sauvignon and Chardonnay grapevines. More recently, comparable thermal-time formulations have accurately represented reproductive phenology in several sweet-cherry cultivars under Mediterranean conditions (Campillay-Llanos et al., 2024). Comparable biomathematical approaches have also been validated for pear (Campillay-Llanos et al., 2025) and European hazelnut (Rosales et al., 2026). Together, these studies support thermal time as a useful physiological clock across fruit-tree species.

Most available models, however, assign a single phenological trajectory to an entire site. Commercial orchards are rarely homogeneous: slope, exposure, soil water availability, canopy vigour, irrigation distribution, and local temperature can generate persistent differences between rows and management blocks. A time-only model cannot explicitly describe these spatial patterns.

Reaction–diffusion equations provide a natural extension. The reaction term retains the local biological development law, while a spatial operator regularises nearby trajectories. In this application diffusion does *not* represent physical movement of plants or phenological stages. It is an effective representation of spatial coherence arising from environmental continuity and shared management.

The objective of this conference paper is to formulate a spatial bioclimatic framework for sweet-cherry phenology, connect it explicitly to the classical monomolecular model, describe a stable numerical implementation, and illustrate its behaviour under observed and warming scenarios.

2. Materials and methods

2.1 Classical thermal-time model

Let $P(t)$ denote a continuous phenological score and let t = GDD be accumulated thermal time. The classical monomolecular model is

$$\frac{dP}{dt} = \beta(\alpha - P), \tag{1}$$

where α is the final or asymptotic phenological stage and $\beta > 0$ is the development rate per unit of thermal time. For $P(0) = P_0$, its solution is

$$P(t) = \alpha - (\alpha - P_0)e^{-\beta t}. \tag{2}$$

Thus, development is rapid when the current state is far from α and slows as the final stage is approached. The fitted values reported for sweet cherry at the study site provide the biologically plausible range

$$\beta \in [0.0033,\ 0.0045]\ (^{\circ}\mathrm{C}\cdot\mathrm{day})^{-1},$$

with coefficients of determination of approximately 0.96–0.98 (Campillay-Llanos et al., 2024).

2.2 Reactive component: biological basis and derivation

The reactive component is the biological core of the proposed framework. It describes the development that would occur at a fixed point in the orchard if that point evolved independently of its neighbours. Its construction begins with a simple physiological assumption: for a given amount of accumulated thermal time, the instantaneous advance is proportional to the fraction of the phenological process that remains to be completed.

Let α denote the upper stage of the interval being modelled and let $P(t) < \alpha$ be the current phenological state. The remaining developmental distance is

$$R(t) = \alpha - P(t). \tag{3}$$

If each additional unit of effective thermal time completes a constant proportion β of this remaining distance, then

$$\frac{dP}{dt} = \beta R(t) = \beta(\alpha - P). \tag{4}$$

This is the monomolecular or Mitscherlich law used in eq. (1). Equivalently, the remaining distance satisfies

$$\frac{dR}{dt} = -\beta R, \tag{5}$$

so the unresolved fraction of the phenological process decreases exponentially:

$$R(t) = R(0)e^{-\beta t}. \tag{6}$$

Substitution of $R(0) = \alpha - P_0$ directly yields eq. (2). This derivation explains why the model is monotone, bounded, and asymptotic without imposing those properties artificially.

2.2.1 Interpretation of the phenological state

The variable P is a continuous representation of an ordered phenological scale. Observed stages are discrete, but the continuous state provides a useful interpolation between field observations. Thus, a value of P between two recorded stages represents progress through the corresponding developmental transition. The parameter α is not a development rate: it is the upper state of the interval. It may represent the last stage of a complete seasonal scale or the terminal stage of a specific phase, such as flowering or fruit development.

The initial value P_0 locates the system at the beginning of the simulated thermal interval. Changing P_0 shifts the trajectory vertically, whereas changing the GDD origin shifts it horizontally. These two operations must be distinguished during calibration: the first represents a different initial biological state and the second a different thermal reference date.

2.2.2 Meaning and sensitivity of the thermal rate

The coefficient β has units $(^{\circ}\mathrm{C}\cdot\mathrm{day})^{-1}$ and determines how efficiently thermal accumulation is converted into phenological progress. A larger β produces an earlier approach to α for the same GDD. The model sensitivity to β is

$$\frac{\partial P(t)}{\partial \beta} = (\alpha - P_0)\, t\, e^{-\beta t} > 0 \qquad (t > 0), \tag{7}$$

which shows that the influence of β is greatest during the transition and declines as the asymptote is approached. This parameter therefore has a direct agronomic interpretation: it distinguishes cultivars, seasons, or orchard sectors that require different amounts of effective thermal time to reach comparable stages.

An especially transparent quantity is the thermal half-time, defined as the GDD required to reduce the remaining developmental distance by one half:

$$t_{1/2} = \frac{\ln 2}{\beta}. \tag{8}$$

For the reference range $\beta \in [0.0033, 0.0045]$, this corresponds approximately to 154–210 GDD. The half-time converts the fitted rate into a quantity that can be discussed directly with crop specialists.

2.2.3 Why GDD is the independent variable

Calendar time alone does not distinguish a warm day from a cool day. Thermal time replaces the calendar clock with a physiological clock. If $T_{min}(d)$ and $T_{max}(d)$ are the daily temperatures, a selected GDD method defines an effective daily contribution g_d relative to the base and upper thresholds, and

$$t_n = \mathrm{GDD}_n = \sum_{d=1}^{n} g_d. \tag{9}$$

The reaction law then states that comparable increments of effective heat produce comparable developmental responses. This separation is valuable: the GDD calculation describes the environmental forcing, while eq. (4) describes the biological response to that forcing.

2.2.4 Local model, calibration, and predictive use

At a fixed location, observations $\{(t_j\ ,\ P_j)\}_{j=1}$ can be used to estimate α, β, and, when necessary, P_0 by nonlinear least squares or likelihood-based methods. The fitted curve can then be inverted to estimate the thermal requirement for any target stage $P^* < \alpha$:

$$t^* = -\frac{1}{\beta}\ln\ \frac{\alpha - P^*}{\alpha - P_0}\quad . \tag{10}$$

Combining t^* with a forecast of thermal accumulation converts the required GDD into a predicted calendar date. This is the practical mechanism through which the reactive model supports planning of flowering observations, crop-protection windows, and harvest operations.

The reaction model is deliberately parsimonious. It is

appropriate when development is monotone over the selected interval and approaches a terminal stage progressively. If observations exhibit several distinct phases, the season can be divided into biologically meaningful intervals or the reaction law can be replaced by a more flexible validated function. Importantly, the spatial extension developed below does not depend on a particular reaction law: the monomolecular component can be retained or substituted without changing the general reaction–diffusion architecture.

2.3 Reaction–diffusion extension

Let $\Omega \subset \mathbb{R}^d$, with d = 1 or 2, represent a row or a two-dimensional orchard. The phenological field $P(x, t)$ satisfies

$$\frac{\partial P}{\partial t} = \beta(\mathbf{x}, t)(\alpha - P) + D\nabla^2 P, \qquad \mathbf{x} \in \Omega,\ t > 0, \tag{11}$$

with initial condition

$$P(\mathbf{x}, 0) = P_0(\mathbf{x}), \tag{12}$$

and homogeneous Neumann conditions

$$\nabla P \cdot \mathbf{n} = 0 \qquad \text{on } \partial\Omega. \tag{13}$$

Here, $D \geq 0$ is an effective spatial-coupling coefficient. When $D = 0$ and β is spatially constant, eq. (11) reduces exactly to eq. (1). Conditions eq. (13) impose no coupling with sectors outside the modelled orchard.

Equation eq. (11) must be read as a collection of local reactive models linked through space. At every position x, the term

$$\beta(\mathbf{x}, t)(\alpha - P(\mathbf{x}, t))$$

advances the local phenological state according to the thermal mechanism derived above. The Laplacian compares that state with its immediate neighbourhood. In one dimension,

$$\nabla^2 P = P_{xx}, \tag{14}$$

and in two dimensions,

$$\nabla^2 P = P_{xx} + P_{yy}. \tag{15}$$

At a local minimum of the phenological field, $\nabla^2 P > 0$ and the coupling term increases the local rate of change; at a local maximum, $\nabla^2 P > 0$ and it reduces that rate. Consequently, diffusion regularises short-scale contrasts while the reaction term continues to drive the entire field towards α.

2.3.1 What diffusion represents in a fixed crop

Phenology itself does not move from one tree to another. Therefore, D must not be interpreted as a physical dispersal coefficient. It is an *effective coupling parameter* that represents spatial coherence produced by shared or smoothly varying conditions: air temperature, solar exposure, soil water availability, canopy continuity, irrigation, cultivar distribution, and management. This distinction is central to the biological interpretation of the model.

The dimensions of D are length^2/(°C·day) because the evolution variable is GDD. A characteristic coupling length over a thermal interval t is

$$\ell_D(t) \sim \sqrt{Dt}. \tag{16}$$

This quantity gives the approximate spatial scale over which local differences are smoothed during the selected amount of thermal development. It also offers a practical way to compare the fitted D with row spacing, sensor spacing, and management-block size.

2.3.2 Why the extension is useful

The classical model predicts *when* a reference phenological stage is reached for an average site. The spatial extension additionally predicts *where* that stage has been reached and how synchronous the orchard is. This distinction enables several applications:

- identifying sectors that enter flowering or fruit development earlier;
- mapping the spatial width of pesticide or frost-protection windows;
- organising repeated observations and targeted sampling;
- coordinating irrigation, thinning, and harvest by management zone;
- comparing whether warming advances all orchard sectors uniformly; and
- distinguishing broad spatial gradients from isolated observational noise.

The model also separates two sources of spatial variability. Heterogeneity in $\beta(x, t)$ represents systematic differences in the local development mechanism. In contrast, D represents the degree of spatial coherence among neighbouring trajectories. Estimating both components is more informative than smoothing observed maps alone because it preserves a mechanistic interpretation: local forcing creates differences and spatial coupling moderates them.

For $P_0(x) \in [0, \alpha]$, $\beta(x, t) \geq 0$, and $D \geq 0$, the parabolic maximum principle ensures that the biologically meaningful interval is invariant:

$$0 \leq P(\mathbf{x}, t) \leq \alpha. \tag{17}$$

This provides a basic consistency requirement for calibration and simulation.

2.4 Bounded heterogeneous development rate

Spatial and seasonal variability is introduced through a bounded logistic mapping,

$$\beta(\mathbf{x}, t) = \beta_{\min} + \frac{\beta_{\max} - \beta_{\min}}{1 + \exp[-\eta(\mathbf{x}, t)]}. \tag{18}$$

In one dimension, a parsimonious smooth predictor is

$$\eta(x, t) = a_0 + \sum_{k=1}^{K} a_k \cos \quad \frac{k\pi x}{L} \quad \sum_{\ell=1}^{L_t} b_\ell \phi_\ell(t), \tag{19}$$

where low-frequency cosine modes capture persistent spatial gradients and ϕ_ℓ are smooth functions of GDD. A zoned alternative assigns different offsets or weights to predefined orchard sectors.

For a rectangular two-dimensional orchard,

$$\eta(x,y,t) = c_0 + \sum_{m=1}^{M}\sum_{n=1}^{N} c_{mn}\cos\left(\frac{m\pi x}{L_x}\right)\cos\left(\frac{n\pi y}{L_y}\right) + \sum_{\ell=1}^{L_t} d_\ell \phi_\ell(t). \quad (20)$$

Low values of K, L_t, M, and N limit overfitting. Management-block effects can be added to eq. (20) when field observations support a zoned structure.

Table I

Variables and parameters in the spatial phenology model.

Symbol	Role	Phenological interpretation
$P(x, t)$	State variable	Continuous phenological score at orchard location x and accumulated thermal time t.
t = GDD	Physiological time	Accumulated growing degree days from a defined starting date.
α	Upper state	Final or asymptotic stage of the modelled phenological interval.
$\beta(x, t)$	Development rate	Local thermal response, bounded by β_{min} and β_{max}.
D	Spatial coupling	Effective strength of spatial coherence among neighbouring orchard sectors.
$\nabla^2 P$	Spatial operator	Local curvature that smooths phenological gradients.
$P_0(x)$	Initial condition	Observed or prescribed spatial phenological state at the start of simulation.

2.5 Thermal data and climate scenarios

The bioclimatic information corresponds to a commercial sweet-cherry orchard in the Maule Region, Chile (34◦49′55″ S, 71◦17′32″ W; 223 m a.s.l.). The region has a Mediterranean climate with a dry summer season. Temperature records from the 2017 and 2020 seasons were used to construct representative thermal trajectories.

Daily GDD were estimated with a single-sine method using a base temperature of 10◦C and an upper threshold of 35◦C, following the phenological modelling procedure used for sweet cherry by Campillay-Llanos et al. (2024). Unlike a simple daily mean, the sine method accounts for days on which temperature crosses a developmental threshold.

A baseline trajectory was obtained from the observed seasons after interpolation to a common seasonal index. Warming scenarios were generated with a delta-scaling approach:

$$\mathrm{GDD}_s(q) = f_s\,\mathrm{GDD}_{\mathrm{base}}(q), \quad (21)$$

$$f_s = \frac{\mathrm{GDD}_{\mathrm{base}}(Q) + \Delta_s}{\mathrm{GDD}_{\mathrm{base}}(Q)}, \quad (22)$$

where q is calendar position within the season, Q is the end of the season, and Δ_s is the scenario-specific increase in total GDD. This exploratory construction preserves the observed intra-seasonal curve shape while changing its magnitude. It does not represent a complete downscaled climate projection.

2.6 Numerical scheme

The orchard domain was discretised on a uniform grid and the Laplacian was approximated by centred second-order finite differences. An implicit–explicit (IMEX) Euler scheme treated reaction explicitly and diffusion implicitly:

$$(I - \Delta t\, DL_h)\, P^{n+1} = P^n + \Delta t\, \boldsymbol{\beta}^n \odot (\alpha\mathbf{1} - P^n), \quad (23)$$

where L_h is the discrete Laplacian, $\odot$ denotes component-wise multiplication, and Δt is measured in GDD. The implicit diffusion step avoids the restrictive parabolic stability condition of a fully explicit scheme. Since $I - \Delta t DL_h$ is constant for a fixed grid and D, a sparse LU factorisation can be computed once and reused.

To preserve non-oscillatory reaction dynamics, the explicit step was selected so that

$$\Delta t \max_{\mathbf{x},t} \beta(\mathbf{x}, t) \le 1. \quad (24)$$

The computed state was also checked against eq. (17); numerical clipping is used only as a safeguard against round-off, not as a substitute for an appropriate time step. All simulations were implemented in MATLAB using sparse matrices. Two-dimensional snapshots were examined near full bloom ($t \approx 141$ GDD) and shuck fall ($t \approx 215$ GDD).

3. Results

3.1 One-dimensional orchard

The one-dimensional simulations reveal how the assumed structure of $\beta(x, t)$ controls within-row synchrony. With low-frequency smooth spatial modes, phenological development changes gradually along the orchard and the diffusion term attenuates small local differences (fig. 1). When three explicit spatial zones are introduced, sharper contrasts emerge in the GDD required to cross phenological thresholds (fig.2). Spatial coupling smooths transitions at zone boundaries but does not erase persistent differences in local development rate.

3.2 Two-dimensional orchard

At the calendar date when the 2017 season reaches approximately 141 GDD, the warmer scenarios have accumulated more thermal time and consequently display more advanced phenological states (figs. 3 and 5). The same mechanism is observed at the 215 GDD reference date associated with shuck fall (figs. 4 and 6). Thus, equal calendar dates do not imply equal physiological time.

The two-dimensional maps retain spatial patterns imposed by heterogeneous development rates across the 3 × 3 management blocks. Diffusion creates continuous transitions, but highand low-rate sectors remain distinguishable. The scenario contrast is stronger at the later stage, because thermal differences have accumulated over a longer period. These results indicate that warming may produce both a general advance and a spatially non-uniform response within the orchard.

Figure 1.
Spatio-temporal phenology in a one-dimensional orchard with a smoothly varying development rate. Panels compare the 2017 and 2020 seasons with RCP 4.5 and RCP 8.5 warming scenarios over a common GDD range. Colours show P(x, t) and contours mark selected phenological levels.

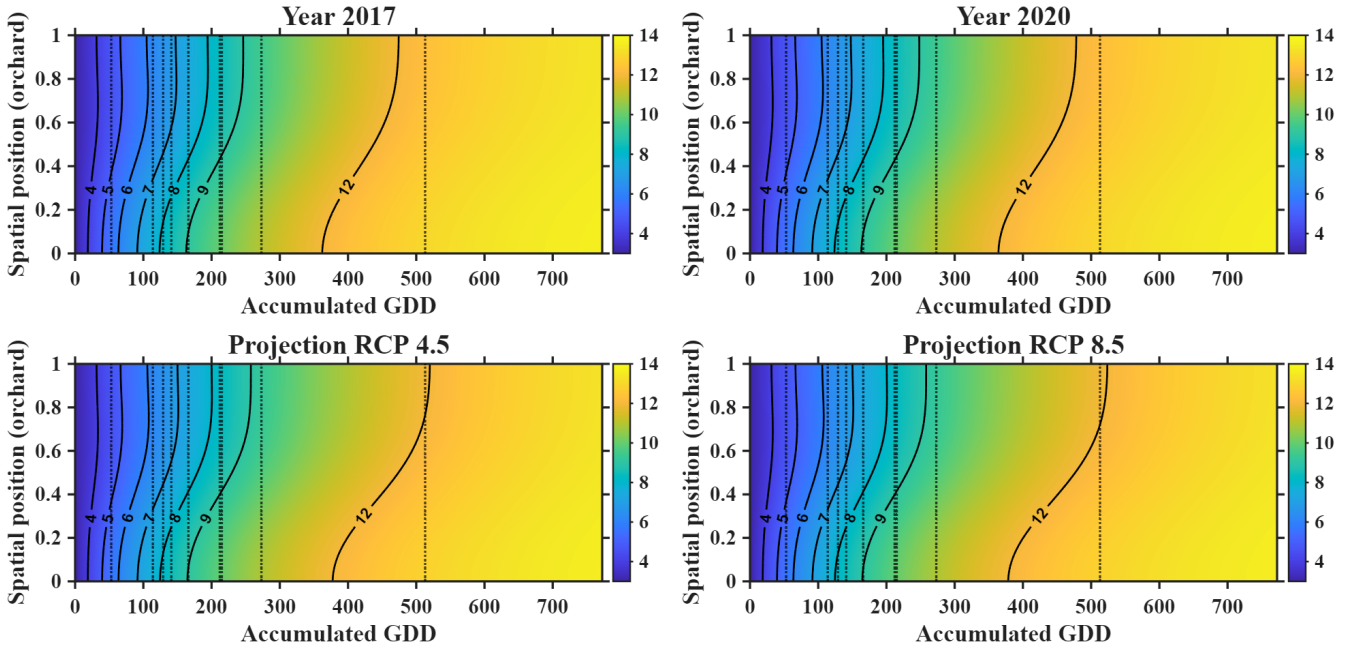

Figure 2.
Spatio-temporal phenology in a heterogeneous one-dimensional orchard with three spatial zones. Zone-specific components of the local development rate produce clearer intrafield asynchrony than the smooth formulation, while diffusion softens transitions between adjacent sectors.

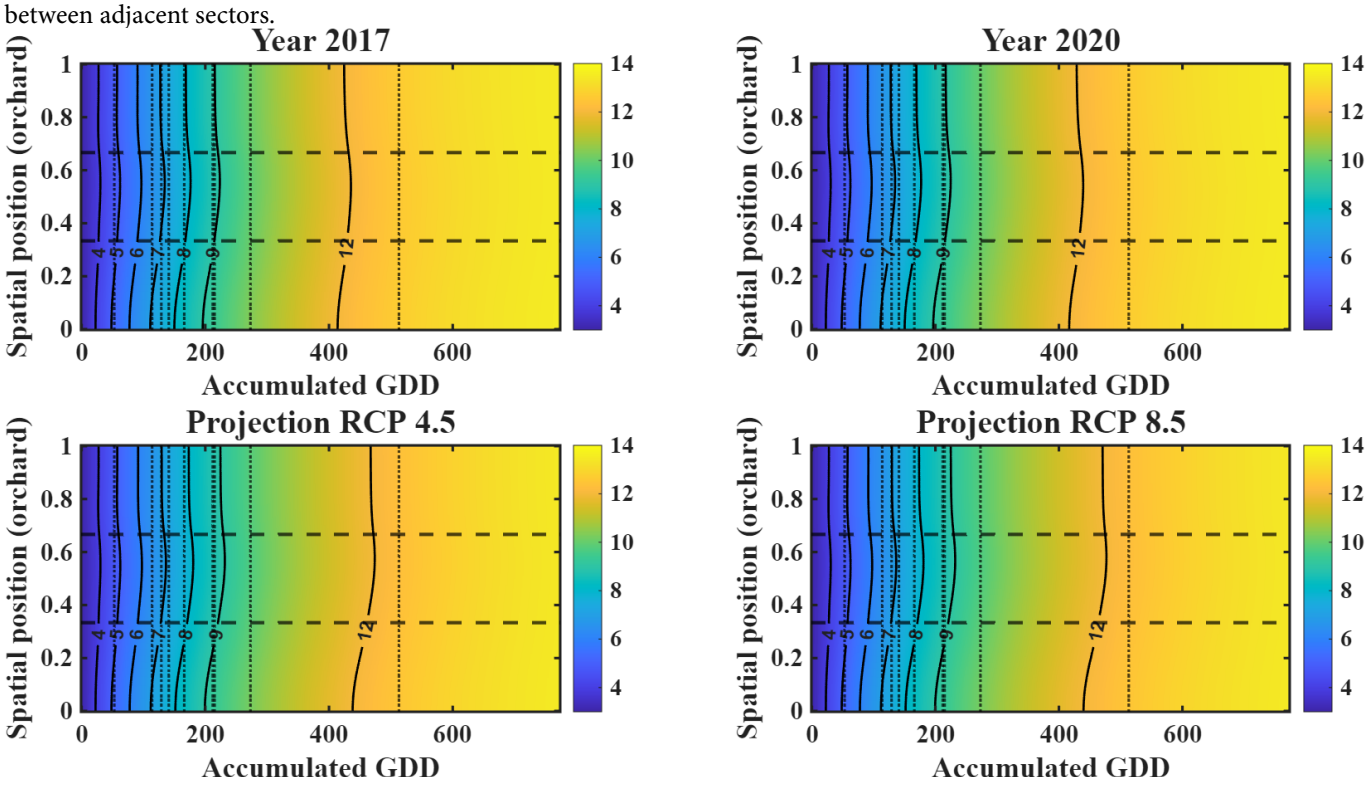

Figure 3.
Two-dimensional reaction–diffusion simulation at the calendar date on which 2017 reaches approximately 141 GDD (full bloom). The same date is used for all scenarios; warmer trajectories therefore correspond to greater effective physiological time. Dotted lines delimit nine orchard blocks.

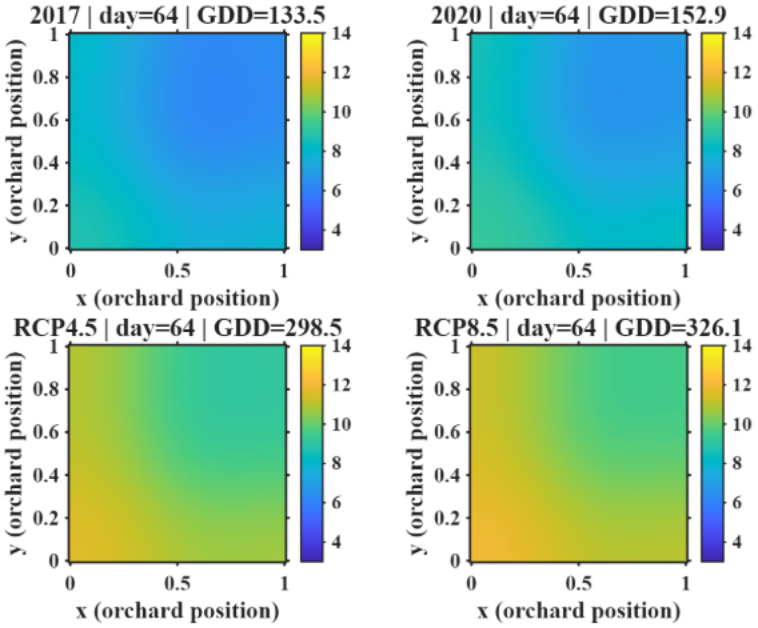

Figure 4.
Two-dimensional reaction–diffusion simulation at the calendar date on which 2017 reaches approximately 215 GDD (shuck fall). Additional thermal accumulation advances the simulated state in the warming scenarios while spatial oupling smooths, but does not eliminate, block-level contrasts.

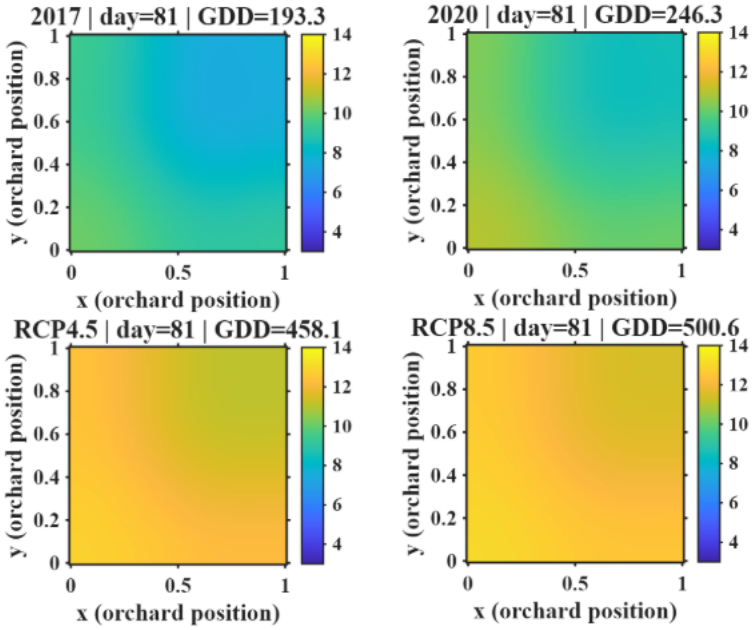

Figure 5.
Full-bloom comparison for the heterogeneous two-dimensional orchard with nine zones. The bounded rate $\beta(x, y, t)$ combines block effects, temporal modulation, and within-zone variability; all panels are evaluated at the same calendar position.

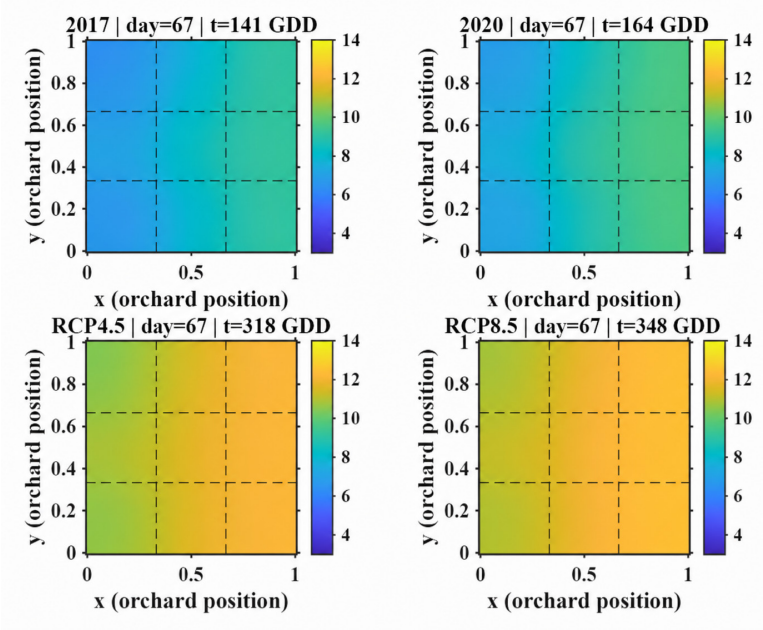

Figure 6.
Shuck-fall comparison for the heterogeneous two-dimensional orchard with nine zones. Laterseason thermal accumulation increases the separation between observed and warming scenarios and reveals persistent spatial differences in development.

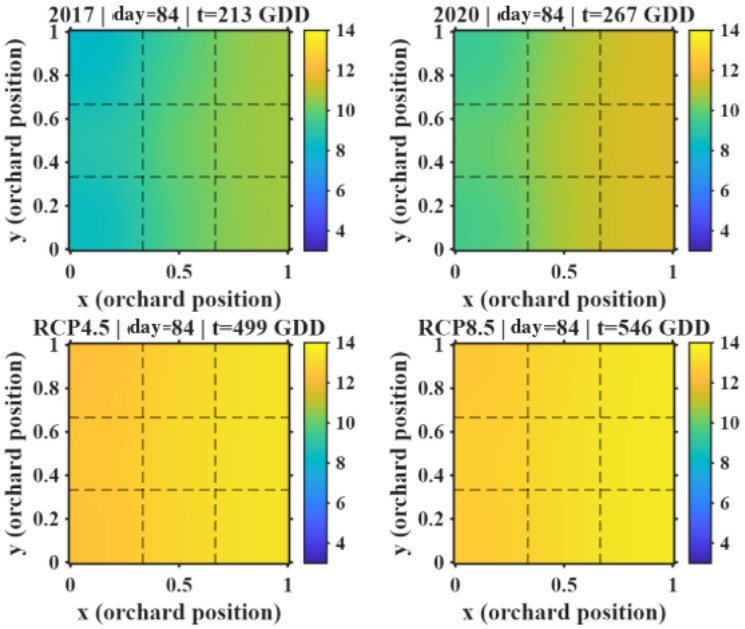

4. Discussion

The proposed framework preserves the interpretability of a validated thermal-time model while adding a spatial state. This is its principal conceptual contribution: the classical trajectory becomes a local reaction law, and orchard heterogeneity enters through $\beta(x, t)$, $P_0(x)$, and a effective spatial-coupling coefficient. The resulting maps can represent asynchronous flowering or maturity that a single orchard-average curve cannot show.

The parameter D requires careful interpretation and calibration. It does not describe movement of phenological material. Instead, it quantifies spatial regularity after measured covariates and block effects have been incorporated. A large fitted D indicates that neighbouring sectors tend to display similar phenological trajectories; a small value permits local differences to persist. Calibration should therefore combine repeated phenological observations with spatially resolved temperature, soil, vigour, and management information.

The framework is compatible with digital agriculture (Basso and Antle, 2020). Phenocams, proximal sensors, unmanned aerial vehicles, and georeferenced field scoring could supply observations for estimating $P(x, t)$ and $\beta(x, t)$. These data would permit formal parameter estimation, uncertainty quantification, and out-of-sample validation. Operationally, predicted maps could support block-specific crop protection, irrigation scheduling, labour allocation, and selective harvest.

Several limitations define the next stage of research. First, the numerical experiments illustrate model behaviour and should not yet be interpreted as a fully calibrated predictive product. Second, the delta method assumes that warming is distributed proportionally through the season and does not represent changes in daily variability, heat waves, or late frosts. Third, the current model uses isotropic and constant D; anisotropic or spatially varying coupling may be more appropriate for row-oriented orchards. Finally, nonlocal operators could represent correlations beyond immediately adjacent grid cells when supported by field data.

5. Conclusions

A classical monomolecular phenological model can be extended coherently to an orchard-scale reaction–diffusion equation. The reaction term retains the thermal-time interpretation of fruittree development, while effective diffusion describes spatial coherence among neighbouring sectors. The IMEX finite-difference formulation provides a stable and computationally efficient implementation in one and two dimensions.

The simulations show that spatially heterogeneous development rates generate persistent within-orchard asynchrony and that warmer thermal trajectories advance phenological state at the same calendar date. With field calibration and spatial validation, the framework can become a practical component of climate-adaptive and site-specific management in sweet-cherry production.

Acknowledgements and Funding

The authors acknowledge the research environments of NIPA–Universidad Católica de Temuco, LIARC–Military Institute of Engineering, and CITRA/PIEI A2C2–Universidad de Talca. This research was partially funded for M.M.L.-F. by project EVAAT-GCN, FINEP agreement 01.24.0661.00, ref. 3311/24.

Declaration of competing interests

The authors declare no competing interests.

References

A. Rosales, S. Ortega-Farías, D. de la Fuente-Sáiz, R. Morales-Zárate, W. Campillay-Llanos, E. Suarez, and M. J. (2026) Lispuerguer, Development of predictive models for simulating vegetative and reproductive phenology in European hazelnut trees (Corylus avellana L.), International Journal of Biometeorology, 70(6) , 184.

B. Basso and J. Antle (2020) Digital agriculture to design sustainable agricultural systems, Nature Sustainability, 3, 254–256. doi:10.1038/s41893-020-0510-0.

S. Ortega-Farías, P. Lozano, Y. Moreno, and L. León (2002) Desarrollo de modelos predictivos de fenología y evolución de madurez en vid para vino cv. Cabernet Sauvignon y Chardonnay, Agricultura Técnica, 62(1), 27–37. 13

W. Campillay-Llanos, S. Ortega-Farías, and L. Ahumada-Orellana (2024) Development and validation of phenological models for eight varieties of sweet cherry (Prunus avium L.) growing under Mediterranean climate conditions, Scientia Horticulturae, 326, 112711. doi:10.1016/j.scienta.2023.112711.

W. Campillay-Llanos, S. Ortega-Farías, G. A. Díaz, L. Ahumada-Orellana, and R. López-Olivari (2025) Phenological analysis through biomathematical models of three varieties of pear (Pyrus communis L.) in Mediterranean climate conditions, Ecological Modelling, 504, 111105. doi:10.1016/j.ecolmodel.2025.111105.